THE ASTROPHYSICAL JOURNAL, 467:61–75, 1996 August 10

THE RELATIONSHIP BETWEEN THE HIGH-ENERGY CONTINUUM AND EMISSION LINES IN QUASARS: A LOW-REDSHIFT SAMPLE

PAUL J. GREEN
Harvard-Smithsonian Center for Astrophysics, 60 Garden Street, Cambridge, MA 02138; pgreen@cfa.harvard.edu
Received 1995 December 29; accepted 1996 March 14

ABSTRACT

Photoionization models dictate that many prominent quasar emission lines are sensitive to both the luminosity and shape of the quasars' high-energy continuum—primarily the extreme ultraviolet (EUV) and soft X-ray continuum. Unfortunately, the EUV band is severely obscured by Galactic absorption. Using data from the adjacent UV and soft X-ray bandpasses, we initiate the first large-scale, multiline investigation of correlations between the QSO soft X-ray continuum and line emission in a sample of QSOs observed by *Einstein* and *IUE*.

We present a new error analysis for objective, automated line measurements, which enables us to include the information contained in weak or undetected lines. We tabulate more than 300 UV emission-line equivalent widths from *IUE* spectra of 85 QSOs in the atlas of Lanzetta, Turnshek, & Sandoval, then characterize the distributions of line equivalent and velocity widths (W_λ and FWHM). We then compare these line parameters to the QSO continuum spectral energy distributions from optical through soft X-ray wavelengths, using survival analysis to incorporate any nondetections for X-ray flux and/or UV emission lines. Several correlations noted in previous studies are *not* reproduced here. However, we illustrate that the exclusion of undetected lines from such studies may spuriously enhance apparent correlations.

We find significant correlations between W_λ and UV luminosity (e.g., the well-studied Baldwin effect) for Lyα, C IV, He II, and C III]. W_λ(C III]) and W_λ(He II) also show previously unreported correlations with X-ray luminosity that, for C III], appears to be primary. The line ratios C III]/Lyα and He II/Lyα both show strongest dependence on l_X. W_λ(Lyα) correlates strongly with spectral slopes α_{UV} and α_{OX} (between 2500 Å and 2 keV), but *not* with X-ray luminosity.

Using these results, we argue that one simple geometrical interpretation of the Baldwin effect (BEff) as a result of a distribution of disk inclinations is not plausible. We also provide evidence that the BEff weakens or disappears when the line emission is correctly compared to the luminosity in the continuum bandpass relevant to its production. We thus support the interpretation of the BEff as a change in spectral energy distribution with luminosity, and we predict that no BEff relative to X-ray luminosity should be found for Fe II or Mg II emission lines. Extensions of our method to samples of a wider redshift/luminosity range will be presented in a later paper, which will test these predictions.

Subject headings: galaxies: active — quasars: emission lines — quasars: general — ultraviolet: galaxies — X-rays: galaxies

1. INTRODUCTION

1.1. *The Ionizing Continuum of Quasars*

The majority of the nearly 8000 quasars known to date were discovered either via their prominent optical and ultraviolet (OUV) emission lines or from their distinct colors in these bandpasses. The production of emission lines in QSO spectra is widely attributed to photoionization and heating of the emitting gas by the UV to X-ray continuum (e.g., Ferland & Shields 1985; Krolik & Kallman 1988). Individual emission lines from a given ion are particularly sensitive to photons of energy above the corresponding ionization threshold. As an example, the continuum flux relevant to the production of Lyα emission is above 13.6 eV, while He II λ1640 is produced by photons above the 54 eV ionization edge of He^+, which at 228 Å is in the EUV. Note, however, that the production of many emission lines may be sensitive to continuum energy ranges both softer and harder than the ionization potential of the species in question, because such photons may ionize from excited states and also heat the gas via free-free and H^- absorption. Many important lines respond to the extreme ultraviolet (EUV) or soft X-ray continuum. Unfortunately, the EUV band is severely obscured by Galactic absorption. However, constraints on the EUV ionizing continuum are available both through analysis of the emission lines and through the adjacent UV and soft X-ray windows.

Both radio-loud (RL) and radio-quiet (RQ) quasars are seen to have soft ($\lesssim$1 keV) X-ray emission that exceeds the extrapolation from the power-law continuum observed at higher energies (e.g., Turner & Pounds 1989; Masnou et al. 1992). This X-ray "soft excess" has often been interpreted as the high-energy continuation of the big blue bump (BBB), possibly thermal emission from the surface of an accretion disk (although see Barvainis 1993). From the optical/UV side, the bump is an upturn in emission toward shorter wavelengths commonly observed in quasar spectral energy distributions (SEDs; e.g., Elvis et al. 1994). Somewhere in the EUV band, the SEDs must peak and turn down again to meet the observed X-ray emission.

1.2. *Emission Lines as Continuum Diagnostics*

There are pressing reasons to investigate the relationship between available measurements of their high-energy continuum and the OUV emission lines in QSOs. The first is to investigate observational constraints on photoionization models for the broad line region (BLR) of active galactic nuclei (AGNs): do spectral energy distributions (SEDs)

directly determine emission-line strengths or line profile parameters? Conversely, do similar emission-line parameters in QSOs provide empirical testimony for similar high-energy SEDs?

The overall similarity of QSO emission-line spectra had been taken as evidence of fairly uniform, robust physical conditions in the BELR, which encouraged the assumption that clouds in the BELR inhabit a narrow swath of parameter space (in density, size, and ionization parameter). Early photoionization pioneers such as Mushotzky & Ferland (1984) ran models on a single cloud. Refinements using cloud ensembles showed a reduced dependence of total line emission on intrinsic QSO SEDs (Binette et al. 1989). Details of individual clouds or even clouds in a single "zone" can be lost in the mix, and correlations between continuum shape and observed line parameters can be diluted. Baldwin et al. (1996) reiterate that averaging of emission from clouds with a wide variety of properties (but uniformly large columns) results in QSO line spectra robustly consistent with those observed. Correlations of W_λ with SED would provide evidence against such models.

Perhaps emission lines can be used to infer the strength and shape of the high-energy SED (Krolik & Kallman 1988; Zheng 1991), even in the presence of extrinsic effects such as absorption along the line of sight. As an example, radio-quiet QSOs with broad UV absorption lines (BALs) are now known to exhibit markedly weak X-ray emission as a class (Green et al. 1995; Green & Mathur 1996). The similarity of emission-line properties in BAL and non–BAL QSOs (Weymann et al. 1991) has been cited as evidence that orientation is the cause of the BAL phenomenon (i.e., *all* radio-quiet QSOs have BAL clouds). If similar emission lines indeed vouch for similar intrinsic high-energy SEDs, then the large observed α_{OX}-values for BAL QSOs are likely to be caused by strong absorption along the line of sight rather than by differences in their intrinsic SEDs. However, the UV and X-ray absorbers have yet to be positively identified as one (e.g., see the techniques of Mathur 1994). Since BAL QSOs *may* be heavily absorbed, the question of whether similar emission lines are testimony for similar intrinsic SEDs must be answered through study of line/continuum correlations in unabsorbed QSOs. The simple question of whether line equivalent width W_λ correlates with α_{OX}, for example, remains to be explored across a range of emission lines and for QSO samples spanning a range of luminosities.

1.3. *The Baldwin Effect and Changes in Continuum Shape with Luminosity*

If the proportionality between line and continuum strength were linear, then diagnostics such as line ratios and equivalent widths would be independent of continuum luminosity. Baldwin (1977) first noticed that in high-redshift quasars, the equivalent width (hereafter W_λ) of the C IV λ1550 emission line in quasars decreases with increasing UV (1450 Å) luminosity. The Baldwin effect (BEff) was also found to be strong for ions such as O VI, N V, He II, C III], Mg II, and Lyα (e.g., Tytler & Fan 1992; Zamorani et al. 1992). Several possible explanations for the BEff have been offered, one being a dependence of blue bump strength on luminosity.

The shape of the continuum (i.e., the SED) of quasars does appear to correlate with luminosity. In the UV regime, Zheng & Malkan (1993) found that the UV continuum increases in strength relative to the optical toward higher luminosities and that the strength of the BEff decreases once the effect of the increasing UV (BBB) continuum is removed. In the X-ray bandpass, the largest, most uniform study—*ROSAT* All-Sky Survey (RASS) observations of 908 QSOs in the Large Bright Quasar Survey (the LBQS/RASS; Green et al. 1995)—confirmed earlier reports (e.g., Wilkes et al. 1994; Tananbaum et al. 1986) that the hypothetical power-law index between UV (rest λ2500) and soft X-ray regimes, α_{OX} increases significantly with luminosity. The increase in α_{OX} is equivalent to a *decrease* in soft X-ray relative to UV emission with increasing luminosity. There are also hints (e.g., Schartel et al. 1996) that the soft X-ray spectral index α_X of QSOs may decrease with luminosity and/or redshift. The decrease in α_X could mean that the soft X-ray spectrum *hardens* with increasing redshift and/or luminosity.[1] Alternatively, a soft excess may shift out of the *ROSAT* passband toward higher redshift and/or move toward lower energies in higher luminosity sources. Any or all of these trends of continuum shape could strongly influence the efficiency of the ionizing continuum and should affect observed emission-line strengths and ratios. Investigations of the relationship between emission-line and continuum strengths abound in the literature, but only a handful of small samples have been studied relating the shape and strength of the *high-energy* QSO continuum to emission lines.

Zheng, Kriss, & Davidsen (1995, hereafter ZKD) find a strong anticorrelation between the W_λ of O VI λ1034 and α_{OX}. Although some models predict such behavior for other UV emission lines, no other such trends have been observed. The increase in α_{OX} with luminosity in QSOs when combined with the observed BEff is not nearly sufficient to explain the trend in W_λ(O VI) with α_{OX}. What might be responsible? Higher luminosity QSOs may undergo spectral evolution such that fewer photons from a soft X-ray excess/BBB component are available for ionization.

The intriguing results of ZKD are based on a variety of published X-ray fluxes, and a heterogeneous compilation of rest-frame UV spectra (two from HUT, 16 from *IUE*, 14 from *HST*, and 29 ground-based), excluding all nondetections. Thus, although they may well prove robust, such results are open to challenge on the basis of the strong, diverse selection effects inherent in such a sample. On the other hand, even in complete, flux-limited samples of QSOs (which often constitute a large fraction of other more heterogeneous samples) there is a strong correlation between redshift and luminosity. At a *given* redshift, the more luminous objects will usually have higher signal to noise (S/N) spectra. As a result, most of the weak-lined QSOs remaining in a sample that ignores nondetections will be luminous (a Malmquist bias). In addition, noise that randomly enhances the apparent line strength will bump low-luminosity objects into the sample with spuriously high-line W_λ (an Eddington bias). Thus, the apparent statistical significance of line/continuum correlations may be spuriously enhanced by a *combination* of selection effects if undetected lines are left out of the sample. Although some general selection effects in line/continuum studies of the BEff have been considered in

[1] Redshift and luminosity dependence can be hard to disentangle in magnitude-limited surveys, but several recent results, e.g., Wilkes et al. (1994), confirm the primacy of (optical) luminosity in the correlation with α_{OX}.

the literature (e.g., Zamorani et al. 1992), few studies can be found incorporating line error estimates and upper limits to line W_λ, both essential to unbiased line/continuum studies.

Here we initiate a line/continuum investigation of wide scope, using (1) large, homogeneous samples, (2) uniform data and analysis, and (3) a wider range of lines and (consequently) ionization potentials. We outline new error analysis for a simple automated line measurement technique (§ 3), and include limits in all analyses. To facilitate further study, we tabulate these data for individual QSOs. Via correlation tests (see § 4 for details), we seek to determine which of l_{UV}, α_{UV}, l_X, or α_{OX} dominates emission-line formation, or at least which parameter most reliably predicts measured line parameters. In combination with other (e.g., higher redshift/luminosity) samples, these data, techniques, and results should prove useful for further studies of the effect of QSO SEDs on the broad emission-line region (BELR). One such follow-up study is now underway, using LBQS and RASS data (Green et al. 1996).

2. SAMPLE

Multiwavelength line/continuum studies are strongly affected by variability. The slope and intensity of optical, UV, and soft X-ray continua are known to vary out of proportion and out of phase to each other and are only occasionally correlated (Reichert et al. 1994; Clavel et al. 1992). Simultaneous multiwavelength coverage is very difficult to obtain and in any case may offer only a slight advantage for understanding the intrinsic physics; emission lines respond to continuum variations with time delays that must be determined separately for each emission line and each object (Reichert et al. 1994; Pogge & Peterson 1992). To compensate for these limitations, we prefer large samples with the most homogeneous data and analysis, and we use averages of multiple exposures whenever practicable. Data sets that permit such averaging are important, since much of the scatter in observed line/continuum correlations like the BEff are caused by variability (Kinney, Rivolo, Koratkar 1990).

2.1. *The UV Spectra*

The *International Ultraviolet Explorer* (*IUE*) satellite has provided several thousand UV spectra of QSOs, BL Lac objects, and Seyferts since its launch. Kinney et al. (1990) selected a subset of 69 of these objects with three or more repeated observations for uniform co-adding, using an optimized extraction technique. Using slightly less restrictive criteria, and similar extraction techniques, Lanzetta et al. (1993, hereafter LTS93) compiled 260 high-quality spectra. They graciously provided these spectra, accompanied by their 1 σ error arrays, so that uncertainties for all measurements can be derived. Continuum fits were also provided. Details of the extraction, dereddening, and continuum fitting techniques are described in LTS93. We exclude BL Lac objects (they generally have no emission lines) and Seyfert galaxies (to avoid aperture effects and contamination from the host galaxy). From the LTS93 compilation, we have selected the subsample of all QSOs (their class 85) with reliable redshifts, yielding 180 objects.

Both metal-line and BAL QSOs are likely to be absorbed in soft X-rays (e.g., Green & Mathur 1996; Mathur 1994), and there is as yet no published soft X-ray study of other absorbed QSOs. We therefore remove from the sample all QSOs with absorbers as listed in Hewitt & Burbidge 1993 (known BALs, measured damped Lyα, optical or UV absorption). We also remove three candidate damped Lya systems from Lanzetta, Wolfe, & Turnshek (1995), leaving 97 objects. Removal of the BAL QSO IRAS 0759+651, and a "possible" BAL 0043+039 (T. Barlow 1995, private communication), leaves an *IUE* sample of 95 QSOs. Since the detection of absorption in any QSO spectrum is dependent on S/N, some absorbed systems probably remain. However, we feel the exclusion of absorbed QSOs where possible enhances our chances of characterizing the *intrinsic* emission line/continuum relationship.

Finally, we remove two QSOs for which none of the emission lines studied here fall into the available *IUE* spectra (1435−015 and 2216−038), and eight QSOs with noisy spectra for which no emission lines are detected (0318−196, 0935+417, 1006+817, 1114+445, 1215+113, 1257+346, 1352+011, and 1402+436). In the final sample of 85 QSOs, both short-wavelength (SWP) and long-wavelength (LW) spectra are available for 62 QSOs. Only SWP spectra are available for 15, and only LW spectra for eight QSOs. The redshifts of our sample range from 0.1 to 2.3, with mean and median $\langle z \rangle$ of 0.55 and 0.36, respectively.

This compilation of high-quality *IUE* spectra of QSOs is necessarily heterogeneous. Many of the QSOs are included simply because they are bright or peculiar in some other waveband. Others have some unique property that warranted their study in the UV. Although the sample is thus not ideal, it could be called representative, since for objects with redshifts $z > 0.05$ in the Hewitt & Burbidge (1993, hereafter HB93) catalog the LTS93 *IUE* sample contains about 85% of all QSOs with $V < 16$, and 50% of those with $V < 17$. More importantly, it is simply the largest low-redshift sample with homogeneous UV spectra currently available.

2.2. *The Soft X-Ray Fluxes*

The quasar database of Wilkes et al. (1994, hereafter WEA94) includes estimates of the X-ray count rates, fluxes, and luminosities for 514 QSOs and Seyfert 1 galaxies observed with the *Einstein* IPC. All objects were previously known via radio or optical selection and most were targets of the X-ray observations. Although like the *IUE* sample the WEA94 targeted sample is heterogeneous, it again represents the largest, most homogeneous data set currently available. By requiring that the QSOs in the *IUE* sample have *Einstein* soft X-ray data available in WEA94, we define the *IUE*/*Einstein* sample of 49 objects.

3. DATA ANALYSIS

With spectra of lower S/N, the use of Gaussian fitting to measure line fluxes and profiles is questionable and tends to leave out the line wings, which in QSOs contain a substantial fraction of the line flux. Another common measurement of line width uses the second moment of the flux about the mean (or median), but it is severely affected by even low-level wings. We therefore measured line parameters from the *IUE* atlas spectra using a summation procedure detailed in Robertson (1986). We integrate line fluxes between rest-frame wavelengths listed in Table 1, using a local linear continuum determined from bands on either side of the emission line. The continuum is taken as the best-fit least-squares line through the mean flux values in these bands. Continuum points more than 3 σ from the mean are

TABLE 1

LINE AND CONTINUUM DEFINITIONS

Line Identification	Line Wavelength (Å)	Integration Limits Line (Å)	Continuum (Å)	Continuum (Å)	Continuum (Å)	Continuum (Å)	Name[a]	Notes
Lyβ + O VI	1025.7 & 1033.8	1018 – 1054	975 – 1018	1056 – 1148	...	...	O VI	1
Lyα + N V	1215.7 & 1240.1	1186 – 1280	1180 – 1190	1280 – 1290	1320 – 1330	1450 – 1480	Lyα	
Si IV + O IV]	1396.7 & 1402.3	1363 – 1443	1320 – 1330	1450 – 1480	1680 – 1700	...	Si IV	
C IV	1549.1	1475 – 1600	1450 – 1480	1680 – 1700	...	...	...	
He II + O III]	1640.5 & 1664.2	1602 – 1680	1450 – 1480	1680 – 1700	...	...	He II	2,3
Al III + C III]	1857.4 & 1908.7	1830 – 1950	1780 – 1830	1970 – 2030	...	...	C III]	3

NOTES.—(1) Both line and continuum region susceptible to Lyα forest contamination; (2) probable contamination from C IV; (3) possible contamination from Fe II.

[a] Shorter name used throughout the text.

iteratively rejected until a maximum of 10 iterations or a minimum of 9 pixels per band has been reached. In the few cases where only one continuum band is covered by the spectrum, we assume a constant continuum level fixed at the mean value of the measurable band. If more than 10% of the line region is missing, no measurement is performed. For spectra with adequate wavelength coverage, our measurement of the equivalent width (W_λ), full width at half-maximum (FWHM), and asymmetry parameter are described in Appendix A. The line measurement errors are estimated directly from the 1 σ error spectrum when available, and otherwise from the noise in the continuum (see Appendix B).

We set a line "detection" threshold of 5 times the errors as computed in Appendix B and include upper limits at that level for lines weaker than the threshold. The largest source of systematic error is the choice of continuum. Our equivalent width measurements may differ systematically from those of other studies, since our measurements are simple and automated. However, they should be internally consistent, and thus most useful for correlation with continuum properties. We consider six UV emission lines (Lyβ + O VI, Lyα + N V, Si IV + O IV], C IV, He II + O III], and Al III + C III). Table 2 lists line equivalent widths and errors for all 85 QSOs in the *IUE* sample. For brevity, and since they show few correlations in this sample with SEDs, we do not present a table of the FWHM measurements. Spectral coverage of Mg II was available for only 10 QSOs, so we do not list these data. Other lines (e.g., C II λ2326) are excluded entirely, since they are generally too weak or blended to detect in spectra of rather low S/N. The shortened names (e.g., O VI rather than Lyβ + O VI) we use throughout the text are indicated in the last column of Table 1.

All luminosities are calculated assuming $H_0 = 50$ km s^{-1} Mpc^{-1} and $q_0 = 0.5$. To derive optical luminosities, we use the B magnitudes listed in WEA94 or HB93. If only V magnitudes are listed, we assume $B-V = 0.3$. We include a reddening correction of $E_{B-V} = \max [0, (-0.055 + 1.987 \times 10^{-22} N_{\rm H}^{\rm Gal}]$ and $A_B = 4E_{B-V}$. The Galactic neutral hydrogen column density, $N_{\rm H}^{\rm Gal}$, is adopted from WEA94. A magnitude-to-flux conversion constant of 48.36 for B magnitudes (Hayes & Latham 1975) yields for the emitted flux at 2500 Å

$$\log [f_{\rm em}(2500)] = -19.34 + \alpha_o \log \left(\frac{2500}{4400}\right) - 0.4(B - A_B + \Delta B) . \quad (1)$$

The correction ΔB includes the effects of both emission lines and continuum slope. We derive ΔB by integrating the B band transmission function over a composite QSO spectrum (Francis et al. 1991). We used a Matthews & Sandage B curve (FWHM = 944 Å, $\lambda_c = 4460$ Å). We provide this k correction in Table 3. For the redshifts relevant to this study, ΔB corresponds well with $\alpha_o = -0.23$, where $f_\nu \propto \nu^{\alpha_o}$.

UV continuum flux and UV spectral slopes are determined using the *IUE* continuum fits of LTS93. Second-order continuum fits to the log-log of these (f_λ) spectra provide the continuum slope $a_{\rm UV}$ and normalization $b_{\rm UV}$. These parameters yield the observed flux

$$\log f^o_{\lambda 1450} = a_{\rm UV} \log \lambda + b_{\rm UV} . \quad (2)$$

The UV spectral slope is $\alpha_{\rm UV} = -2 - a_{\rm UV}$. The rest-frame monochromatic flux at λ1450, $f_{\rm UV}$, is then given by

$$\log f_{\rm UV} = \log f^o_{\lambda 1450} + (1 + \alpha_{\rm UV}) \log (1 + z) . \quad (3)$$

Einstein broadband (0.16–3.5 keV) fluxes corresponding to $\alpha_{\rm X} = -0.5$ were taken from WEA94 (who prefer the convention $f_\nu \propto \nu^{-\alpha_{\rm x}}$). This value of $\alpha_{\rm X}$ is most appropriate for RL QSOs. RL QSOs on average have flatter X-ray spectral indices $\alpha_{\rm X}$ (Wilkes & Elvis 1987; Schartel et al. 1996). Published spectral fits to the *Einstein* data are only available for about 18 QSOs in our sample. The assumption of a mean spectral index $\alpha_{\rm X} = 0.5$ translates (via the X-ray counts to flux conversion factor and k correction) into errors of $\lesssim 30\%$ in the 2 keV X-ray luminosity $l_{\rm X}$. The slope $\alpha_{\rm OX}$ is for a hypothetical power law connecting rest frame 2500 Å and 2 keV, so that $\alpha_{\rm OX} = 0.384 \log (l_{\rm opt}/l_{\rm X})$. Objects with large $\alpha_{\rm OX}$ thus have stronger optical emission relative to X-ray. We tested an analogous quantity, $\alpha_{\rm UVX}$, defined similarly between 1450 Å and 2 keV. We find that $\alpha_{\rm UVX}$ is so tightly correlated with $\alpha_{\rm OX}$ that its use as an alternative or complementary measure of QSO SEDs is probably not warranted. This is because the UV is nearly 100 times closer to the optical than to the soft X-ray bandpass. Our characterizations of continuum spectral energy distributions are presented in Table 4.

Although more than half of the *IUE* sample consists of radio-loud (RL) QSOs, we do not separate these from radio-quiet (RQ) QSOs in this study. Except for reports of differences in C IV asymmetries (Corbin & Francis 1994), the emission-line spectra of RL and RQ QSOs are very similar (Steidel & Sargent 1991; Corbin 1992). Such asymmetry differences may also persist between core and lobe-dominant RL QSOs (Brotherton et al. 1994). The largest problem may be variability. However, the *IUE* spectra are

TABLE 2

ULTRAVIOLET EMISSION-LINE EQUIVALENT WIDTHS[a]

Name	Lyβ + O VI	err	Lyα + N V	err	Si IV + O IV]	err	C IV	err	He II + O III]	err	Al III + C III]	err
0026+129	...	...	59.0	1.8	< 6.1	...	32.7	1.0	18.3	0.6	< 29.6	...
0044+030	< 11.3	...	63.4	6.4	50.3	5.5	50.8	1.8	9.8	0.6	27.9	1.5
0052+251	...	...	91.4	2.6	8.0	1.6	119.1	2.5	15.7	0.9	< 82.5	...
0117+213 [l]	10.2	1.4	27.6	1.5	...	...	...	...	...	...	...	...
0119−286	...	...	89.8	4.3	33.5	2.8	76.3	2.7	12.2	0.9	< 36.0	...
0134+329	< 12.6	...	< 13.1	...	13.9	2.0	< 133.3	...	< 35.4	...	19.3	2.6
0205+024	...	...	52.8	4.4	< 5.1	...	38.5	1.2	9.5	0.6	< 33.2	...
0312−770	24.7	1.1	72.6	2.5	5.3	0.9	69.7	1.1	< 563.5	...	< 139.5	...
0405−123	4.1	0.3	50.1	0.8	< 6.9	...	25.7	1.1	3.0	0.5	5.9	0.7
0414−060	9.0	0.5	109.1	6.9	12.9	1.8	57.9	1.9	9.4	1.4	...	...
0558−504	...	...	27.8	0.8	< 2.7	...	23.1	0.5	10.2	0.3	< 14.9	...
0624+691	7.2	0.6	60.9	1.4	< 1.5	...	51.3	6.5	< 16.1	...	12.2	0.9
0736+017	...	...	132.5	10.1	< 14.5	...	94.5	3.2	< 681.9	...	< 125.8	...
0743−673 [l]	6.3	1.2	57.2	3.1	...	...	...	...	...	...	...	...
0804+761	...	...	101.8	2.8	28.0	1.1	81.7	1.6	19.3	0.5	63.7	4.2
0837−120	...	...	87.6	5.5	< 13.9	...	91.4	2.5	< 32.1	...	< 39.8	...
0859−140 [l]	< 193.0	...	< 78.5	...	...	...	...	...	...	...	...	...
0906+484	...	...	59.9	3.0	< 11.1	...	52.4	2.2	14.8	1.0	< 38.6	...
0953+414 [s]	24.9	1.3	63.8	2.8	8.9	0.9	53.6	1.1	...	...	...	...
1001+291	< 4.5	...	34.1	2.3	5.6	0.7	< 14.4	...	< 14.1	...	20.1	2.1
1004+130	< 5.6	...	9.1	1.5	12.0	1.0	< 100.2	...	<1939.9	...	< 69.1	...
1007+417	< 7.0	...	79.1	4.9	< 21.8	...	72.5	2.8	8.3	1.0	< 6.2	...
1008+133 [l]	< 7.6	...	17.9	1.7	180.7	31.3	...	...	...	...	...	...
1011−282 [s]	17.1	3.2	116.5	12.7	< 11.7	...	...	...	...	...	...	...
1012+008 [s]	...	...	72.9	4.2	< 9.8	...	13.3	1.4	< 3.7	...	...	...
1048−090	< 24.4	...	76.1	13.0	62.9	7.1	< 85.0	...	< 45.5	...	18.3	3.4
1049−005	< 26.6	...	83.9	10.0	< 8.1	...	< 124.9	...	< 78.4	...	18.6	3.5
1100+772	7.6	0.6	60.4	1.5	3.5	0.5	89.9	5.6	< 18.1	...	12.4	2.0
1103−006	< 13.0	...	37.3	2.4	< 12.9	...	27.7	3.9	< 10.2	...	20.7	1.6
1104+167 [l]	...	...	83.4	12.2	< 20.5	...	85.1	3.9	13.8	1.1	< 11.5	...
1116+215	...	...	62.9	1.3	< 2.6	...	36.5	0.5	< 1.2	...	31.2	2.8
1127−145 [s]	...	...	...	...	...	...	...	...	...	...	...	...
1136−135	< 4.7	...	63.5	1.6	< 17.6	...	50.7	3.1	6.7	1.0	20.0	1.0
1137+660	13.9	1.0	74.4	7.9	41.4	7.2	45.9	3.9	< 9.7	...	< 28.4	...
1146−037	< 463.7	...	< 44.4	...	< 43.2	...	268.1	33.5	< 24.5	...	51.8	5.0
1148+549	< 6.3	...	54.6	2.3	11.3	1.2	18.0	1.6	< 22.9	...	...	...
1151+117	...	...	112.0	7.2	< 12.7	...	69.6	2.6	21.8	1.5	< 36.6	...
1156+295	< 1.9	...	< 15.6	...	8.8	1.6	< 5.7	...	< 3.9	...	...	...
1156+631 [l]	...	...	< 133.4	...	< 28.8	...	91.3	7.8	< 11.2	...	< 14.3	...
1202+281	...	...	74.2	1.3	< 3.5	...	129.1	1.2	18.9	0.4	< 35.4	...
1206+459	< 17.6	...	44.5	2.1	< 10.5	...	...	...	...	...	...	...
1216+069	10.1	1.7	53.9	3.9	9.3	1.4	65.0	10.3	< 24.7	...	14.1	2.2
1241+176	8.0	0.9	45.4	0.5	< 6.3	...	...	...	...	...	...	...
1248+401	< 17.1	...	39.6	2.5	< 8.7	...	< 35.3	...	...	...	...	...
1259+593	< 7.1	...	26.8	1.1	< 27.7	...	58.6	8.6	12.2	2.2	16.6	1.0
1302−102	< 1.5	...	42.9	0.8	4.4	0.3	15.9	1.8	< 9.7	...	16.6	1.0
1307+085	...	...	76.1	3.4	< 8.1	...	93.7	1.9	18.8	0.8	< 31.1	...
1309+355 [s]	...	...	46.7	2.3	< 4.9	...	32.9	1.0	< 2.6	...	...	...
1317+277	5.9	1.1	27.0	1.0	3.0	0.4	26.5	1.2	...	...	...	...
1318−113 [s]	...	...	...	...	...	...	...	...	...	...	...	...
1333+176	< 9.8	...	28.5	2.2	< 83.6	...	42.2	6.4	< 9.9	...	7.8	1.5
1334+246	...	...	54.4	5.3	< 25.2	...	63.4	6.6	39.7	2.3	< 133.2	...
1338+416	< 10.7	...	25.8	1.0	26.4	1.8	...	...	...	...	...	...
1352+183	...	...	71.0	3.2	< 7.0	...	85.5	2.3	17.0	1.0	35.8	6.5
1354+195 [s]	17.9	1.5	...	...	...	...	...	...	...	...	...	...
1355−416 [s]	14.8	2.1	63.7	3.7	11.7	1.1	...	...	...	...	...	...
1356+581 [s]	...	...	...	...	...	...	...	...	...	...	...	...
1415+451 [s]	...	...	117.0	7.0	42.2	3.7	80.3	3.4	17.9	1.1	...	...
1425+267	< 18.9	...	51.3	3.4	40.5	2.2	131.3	19.7	< 37.7	...	35.1	3.8
1444+407 [s]	< 3.5	...	51.3	2.2	14.0	0.9	...	...	...	...	...	...
1512+370	7.6	0.5	57.0	0.8	3.5	0.3	83.7	3.6	17.4	1.7	15.2	0.7
1522+101	< 6.3	...	41.2	1.6	...	...	...	...	...	...	...	...
1525+227	< 10.5	...	40.1	6.4	< 7.8	...	< 32.7	...	< 63.4	...	< 51.2	...
1526+285	23.7	4.7	120.9	6.3	< 182.4	...	< 316.5	...	< 99.3	...	< 37.5	...
1538+477	8.1	0.8	75.8	10.0	19.8	2.7	41.7	1.7	11.5	1.1	...	...
1545+210	< 6.6	...	58.1	3.6	< 7.4	...	79.9	5.1	< 35.6	...	< 19.6	...
1552+085	...	...	78.7	9.0	< 20.4	...	210.3	22.1	46.3	4.0	< 142.4	...
1612+261 [s]	...	...	135.7	11.1	22.0	4.4	148.7	6.4	25.1	1.7	...	...
1617+175 [l]	...	...	...	...	...	...	...	...	...	...	41.2	7.6
1630+377	3.5	0.6	39.5	1.0	...	...	...	...	...	...	...	...

TABLE 2—*Continued*

Name	Lyβ + O VI	err	Lyα + NV	err	Si IV + OIV]	err	C IV	err	He II + O III]	err	Al III + C III]	err
1634+706	2.3	0.2	44.0	0.4	...	...	...	...	...	...	...	...
1641+399	9.0	1.0	54.5	3.5	< 14.5	...	33.8	1.8	4.0	0.7	< 5.2	...
1656+053 [c]	< 7.4	...	...	...	...	...	...	...	...	...	...	...
1718+481	< 6.3	...	33.9	0.6	5.4	0.9	...	...	...	...	...	...
1721+343	30.2	1.2	126.3	4.2	< 3.6	...	94.0	1.4	< 11.0	...	18.6	3.0
1803+676	...	...	95.8	3.7	9.6	0.8	133.3	1.3	15.8	0.4	34.4	4.6
1850−782 [b]	...	...	...	...	...	...	...	...	...	...	< 140.0	...
1928+738	7.8	1.3	71.3	3.4	9.1	1.1	< 76.0	...	< 85.9	...	22.7	3.7
2112+059	35.7	6.5	68.9	2.8	< 60.6	...	< 136.0	...	< 23.8	...	30.8	1.7
2141+175 [c]	7.1	1.1	48.1	2.5	7.3	1.1	18.2	0.9	...	...	...	...
2201+315	9.7	0.8	44.1	1.5	16.1	0.6	45.9	3.8	25.7	4.1	9.0	1.7
2251+113	< 19.0	...	28.2	2.8	< 5.2	...	79.8	9.3	< 40.1	...	47.8	3.8
2251+158 [c]	14.5	2.6	...	...	...	...	...	...	...	...	...	...
2302+029	< 9.3	...	12.6	1.7	< 6.0	...	< 33.9	...	...	...	...	...
2344+092	26.1	1.9	58.6	5.7	< 17.6	...	32.3	2.2	< 6.4	...	< 58.6	...

[a] Equivalent widths expressed in Å, in the rest frame.
[b] Only LW spectra available.
[c] Only SWP spectra available.

averaged over a variety of timescales, as are some of the *Einstein* IPC fluxes.

4. RESULTS

4.1. *UV Emission-Line Parameters, and Correlations Between Them*

The sample median and mean (with its error) of emission-line W_λ and FWHM, and of continuum parameters, are listed in Table 5. These were determined using the survival analysis package ASURV (LaValley, Isobe, & Feigelson 1992). We thus incorporate the information in nondetections, which may constitute more than 50% of the data in some cases (e.g., for Si IV + O IV). In survival analysis, the median is always well defined. If, however, the lowest (highest) point in the data set is an upper (lower) limit, the mean is not well defined, since the distribution is not normalizable, and so the outlying censored point is redefined as a detection in our analyses. In Table 5, for these cases we list the value of that redefined limit, where the distribution is truncated.

Our method yields EW distributions quite similar to those of other studies (e.g., Baldwin, Wampler, & Gaskell 1989; Cristiani & Vio 1990; Francis et al. 1991; Laor et al. 1995). As a further means of comparison, we have measured the LBQS composite spectrum of Francis et al. (1991) using our technique, and find equivalent widths of 5.5, 49.7, 9.3, 31.0, 6.9, and 19.9 for O VI, Lyα, Si IV, C IV, He II, and C III], respectively. Our measurements yield W_λ that are 0.93 ± 0.07 times those found by Francis et al. From this figure we exclude a comparison of W_λ(He II) (our W_λ-value is 58% of theirs), since we use a higher continuum estimate for this line. Because of the existence of the BEff, we should not expect our measured mean W_λ measurements to be the same in the *IUE* sample as in other samples, unless their $\langle z \rangle$ and $\langle \log l_{UV} \rangle$ are similar.

Among the emission lines, we find a strong three-way correlation among W_λ(C IV) W_λ(Lyα), and W_λ(He II). For all other parameter pairs showing significant correlations in *both* Spearman rank and generalized Kendall rank tests, we display the best-fit regressions in Table 6 whenever the number of emission-line measurements exceeds 30. Measured FWHM for each line correlates strongly with the W_λ of that line. We note also a significant correlation between C III]/C IV and FWHM(O VI). However, since this is based on only 22 data points (including 13 limits), we postpone discussion to a later paper. We do not confirm significant correlations between C IV/Lyα and C III]/C IV (Mushotzky & Ferland 1984), or between FWHM(C III]) and FWHM (C IV) (Corbin & Francis 1994).

4.2. *SED Parameters, and Correlations between Them*

As expected (given the predominance of magnitude-limited samples), luminosities in different wavebands correlate strongly with one another. Distance-independent parameters such as α_{ox} generally show more scatter. We do

TABLE 3

ADOPTED *B* MAGNITUDE *k* CORRECTIONS[a]

z	ΔB	z	ΔB	z	ΔB	z	ΔB	z	ΔB
0.0	0.000	0.7	−0.511	1.4	−0.733	2.1	−0.832	2.8	−0.724
0.1	−0.071	0.8	−0.529	1.5	−0.772	2.2	−0.870	2.9	−0.669
0.2	−0.171	0.9	−0.545	1.6	−0.811	2.3	−0.894	3.0	−0.607
0.3	−0.259	1.0	−0.574	1.7	−0.822	2.4	−0.879	3.1	−0.541
0.4	−0.349	1.1	−0.631	1.8	−0.828	2.5	−0.849	3.2	−0.466
0.5	−0.421	1.2	−0.671	1.9	−0.827	2.6	−0.813	3.3	−0.378
0.6	−0.475	1.3	−0.703	2.0	−0.823	2.7	−0.772	3.4	−0.278

[a] From LBQS composite spectrum, for a Mathews & Sandage *B* filter.

TABLE 4

CONTINUUM ENERGY DISTRIBUTIONS

Name	z	B	F_x[a]	N_H[b]	α_{uv}[c]	b_{uv}[d]	log l_{opt}[e]	log l_x[f]	log l_{uv}[g]	α_{ox}
0026+129	0.142	14.95	905	4.6	−0.7	−11.5	30.54	26.89	30.12	1.40
0044+030	0.624	15.97	97	2.9	−0.5	−12.5	31.28	27.20	31.09	1.57
0052+251	0.155	15.42	910	4.6	−1.4	−9.2	30.42	26.97	30.27	1.33
0117+213	1.493	16.05	< 170	4.8	−0.2	−13.9	32.03	< 28.19	31.25	> 1.48
0119−286	0.117	14.89	...	1.6	−1.3	−9.5	30.34	...	30.15	...
0134+329	0.367	16.62	410	4.6	−1.1	−11.0	30.65	27.37	30.30	1.26
0205+024	0.156	15.67	660	3.3	−0.8	−11.4	30.29	26.84	30.05	1.32
0312−770	0.223	16.26	510	7.5	−1.2	−10.1	30.48	27.03	30.42	1.32
0405−123	0.574	14.75	685	3.7	−1.1	−9.9	31.73	27.98	31.64	1.44
0414−060	0.781	16.24	230	5.1	−0.5	−12.5	31.44	27.77	31.12	1.41
0558−504	0.137	15.18	...	5.4	−1.3	−9.5	30.44	...	30.25	...
0624+691	0.370	14.50[v]	...	7.0	−0.7	−11.3	31.58	...	31.17	...
0736+017	0.191	16.90	235	9.4	−0.9	−11.4	30.16	26.56	29.84	1.38
0743−673	1.510	16.61	...	11.8	0.0	−14.4	32.04	...	31.31	...
0804+761	0.100	15.15	1400	3.1	−0.1	−13.0	30.11	26.78	30.07	1.28
0837−120	0.198	15.78	1200	5.9	−1.0	−10.9	30.52	27.30	30.12	1.24
0859−140	1.327	16.79	129	5.7	−0.4	−13.2	31.68	27.97	31.13	1.42
0906+484	0.118	16.46	38	1.8	−1.4	−9.6	29.72	25.36	29.60	1.68
0953+414	0.239	14.80[v]	...	1.3	−1.5	−8.6	30.97	...	30.81	...
1001+291	0.329	15.62	...	1.9	−1.6	−8.8	30.90	...	30.81	...
1004+130	0.241	15.93	< 26	3.7	−0.5	−12.5	30.55	< 25.81	30.23	> 1.82
1007+417	0.611	16.80[v]	...	1.2	−1.1	−10.5	30.93	...	31.15	...
1008+133	1.287	16.24	< 37	3.8	−0.4	−12.9	31.81	< 27.40	31.41	> 1.69
1011−282	0.253	16.80	230	5.7	−1.3	−10.2	30.31	26.80	30.14	1.35
1012+008	0.185	16.30[v]	...	3.5	−1.2	−10.5	30.18	...	29.82	...
1048−090	0.344	16.00	440	3.2	−1.3	−10.1	30.80	27.35	30.40	1.33
1049−005	0.357	16.25[v]	...	3.9	−0.5	−12.6	30.75	...	30.33	...
1100+772	0.311	15.86	580	3.0	−1.1	−10.2	30.77	27.38	30.70	1.30
1103−006	0.426	16.39	...	4.1	−1.0	−11.0	30.84	...	30.61	...
1104+167	0.634	15.91	...	1.5	−1.0	−11.1	31.32	...	30.96	...
1116+215	0.177	15.17	710	1.3	−1.0	−10.1	30.57	26.98	30.72	1.38
1127−145	1.187	17.17	150	4.1	−1.4	−10.3	31.38	27.94	31.24	1.32
1136−135	0.557	16.15	...	3.5	−1.6	−9.0	31.14	...	31.19	...
1137+660	0.646	16.50	335	1.0	−1.0	−10.8	31.10	27.77	31.19	1.28
1146−037	0.341	16.96	530	2.5	−0.8	−12.4	30.40	27.42	29.64	1.14
1148+549	0.969	16.12[v]	...	1.2	−1.0	−10.9	31.60	...	31.62	...
1151+117	0.176	15.81[v]	...	2.5	−0.8	−11.5	30.31	...	30.07	...
1156+295	0.729	14.80	...	1.6	−0.4	−12.9	31.88	...	31.05	...
1156+631	0.594	17.10[v]	...	1.9	−1.0	−11.0	30.79	...	30.81	...
1202+281	0.165	15.02	870	1.7	−0.9	−11.2	30.58	27.01	29.83	1.37
1206+459	1.158	16.09[v]	...	1.3	0.1	−14.9	31.75	...	30.78	...
1216+069	0.334	15.68	300	1.6	−1.1	−10.6	30.89	27.15	30.62	1.43
1241+176	1.273	15.38	55	1.8	0.2	−15.3	32.11	27.56	30.77	1.75
1248+401	1.030	16.36[v]	...	1.4	−0.5	−12.7	31.56	...	31.10	...
1259+593	0.472	15.90[v]	...	1.4	−0.9	−11.0	31.08	...	30.96	...
1302−102	0.286	15.09	540	3.4	−0.8	−11.1	31.02	27.28	30.78	1.44
1307+085	0.155	15.28	840	2.1	−1.1	−10.1	30.42	26.94	30.17	1.34
1309+355	0.184	15.75[v]	...	1.0	−1.2	−10.3	30.37	...	29.93	...
1317+277	1.022	16.12	...	1.2	−0.4	−12.9	31.65	...	31.39	...
1318−113	2.308	17.81	...	2.8	−1.7	−9.5	31.64	...	31.98	...
1333+176	0.554	15.64	49	1.8	−0.9	−11.3	31.31	26.80	31.02	1.73
1334+246	0.107	15.30[v]	...	1.1	1.1	−18.2	30.10	...	28.79	...
1338+416	1.219	16.38[v]	...	0.9	0.0	−14.5	31.68	...	30.88	...
1352+183	0.152	15.71	530	2.0	−1.4	−9.5	30.23	26.72	29.90	1.35
1354+195	0.720	16.48	...	2.2	−0.4	−13.1	31.20	...	30.82	...
1355−416	0.313	15.76	620	6.2	−0.5	−12.3	30.92	27.41	30.54	1.35
1356+581	1.371	17.32	...	1.4	−0.8	−12.4	31.40	...	31.05	...
1415+451	0.114	16.04[v]	...	1.1	−1.0	−11.0	29.86	...	29.44	...
1425+267	0.362	15.67	73	1.7	−0.4	−13.1	30.96	26.61	30.16	1.67
1444+407	0.267	16.25[v]	...	1.3	−1.0	−10.8	30.48	...	30.38	...
1512+370	0.371	15.48	350	1.4	−1.4	−9.6	31.05	27.31	30.75	1.44
1522+101	1.321	16.04[v]	...	2.9	0.1	−14.4	31.88	...	31.31	...
1525+227	0.253	16.79	38	4.2	−0.6	−12.2	30.27	26.02	30.16	1.63
1526+285	0.450	16.00[v]	...	2.6	−1.2	−10.5	31.00	...	30.57	...
1538+477	0.770	16.31[v]	...	1.6	−0.1	−13.8	31.33	...	30.88	...
1545+210	0.264	16.05	780	4.3	−1.2	−10.3	30.60	27.37	30.36	1.24
1552+085	0.119	16.02	20	3.4	−0.1	−13.8	29.92	25.08	29.41	1.86
1612+261	0.131	16.00	710	4.1	−1.0	−11.2	30.03	26.72	29.53	1.27
1617+175	0.114	15.53	285	4.1	−1.4	−9.4	30.10	26.20	29.93	1.50
1630+377	1.471	16.26[v]	...	1.1	0.0	−14.3	31.87	...	31.30	...
1634+706	1.334	14.90	93	4.6	−0.2	−12.9	32.40	27.83	31.92	1.75

TABLE 4—*Continued*

Name	z	B	F_x [a]	N_H [b]	α_{uv} [c]	b_{uv} [d]	log l_{opt} [e]	log l_x [f]	log l_{uv} [g]	α_{ox}
1641+399	0.595	18.70	527	1.0	−0.2	−13.4	30.15	27.90	30.84	0.86
1656+053	0.887	17.00	360	6.1	−0.8	−11.6	31.28	28.07	31.21	1.23
1718+481	1.084	15.63[v]	...	2.3	−0.3	−12.9	31.89	...	31.74	...
1721+343	0.206	16.80[v]	1700	3.0	−1.4	−9.2	30.06	27.49	30.51	0.99
1803+676	0.136	16.04	330	4.7	−0.9	−11.1	30.07	26.42	29.91	1.40
1850−782	0.162	15.80[v]	...	9.0	0.1	−14.6	30.45	...	29.50	...
1928+738	0.302	16.80[v]	...	7.8	−1.2	−10.1	30.52	...	30.57	...
2112+059	0.466	18.90	< 61	6.5	−0.9	−11.3	29.99	< 26.75	30.82	> 1.24
2141+175	0.213	15.91	165	8.2	−1.4	−9.4	30.61	26.51	30.50	1.57
2201+315	0.297	15.56	535	9.0	−1.4	−9.2	31.04	27.30	30.98	1.44
2251+113	0.323	16.25	< 63	5.1	−1.2	−10.2	30.71	< 26.44	30.45	> 1.64
2251+158	0.859	16.57	475	6.4	−0.6	−12.3	31.44	28.17	30.99	1.26
2302+029	1.044	16.33[v]	...	5.2	−0.3	−13.2	31.66	...	31.26	...
2344+092	0.672	16.08	180	5.8	−1.2	−10.5	31.39	27.53	31.02	1.48

[a] Flux in 0.16–3.5 keV bandpass, in ergs cm^{-2} s^{-1} from Wilkes et al. 1994, assuming $\alpha_X = -0.5$.
[b] Galactic column density in 10^{20} cm^{-2}.
[c] UV spectral slope ($f_\nu \sim \nu^{\alpha_{UV}}$).
[d] UV normalization (see text).
[e] Log rest-frame luminosity in ergs cm^{-2} s^{-1} Hz^{-1}, at 2500 Å.
[f] Log rest-frame luminosity in ergs cm^{-2} s^{-1} Hz^{-1}, at 2 keV.
[g] Log rest-frame luminosity in ergs cm^{-2} s^{-1} Hz^{-1}, at 1450 Å.

find a significant anticorrelation in the *IUE/Einstein* sample of α_{OX} with X-ray luminosity ($P = 0.18\%$, with slope -0.13). Quoted probabilities here and in Table 6 are for the assumption of a null hypothesis (no correlation) using a Generalized Spearman Rank (ASURV). Similar trends have been noted previously for low-redshift samples (e.g., Corbin 1993; Wang, Brinkmann, & Bergeron 1996).

In the *IUE/Einstein* sample, the positive correlation between α_{OX} and log l_{opt} observed in larger samples (e.g., Green et al. 1995; WEA94; Tananbaum et al. 1986) is seen

TABLE 5

UNIVARIATE DISTRIBUTIONS

Parameter	Sample N_{total}	Sample N^a_{limits}	Median	Mean	RMS	Trunc?	N^b_{del}
Continuum Parameters							
log l_{opt}	85	0	30.87	30.91	0.07	N	
log l_{uv}	85	0	30.71	30.62	0.07	N	
log l_x	49	5	27.07	27.02	0.11	N	
α_{uv}	85	0	−1.09	−1.19	0.06	N	
α_{ox}	49	5	1.38	1.43	0.03	N	
Equivalent Widths W_λ (Å)							
O VI	57	29	6.9	5.9	0.9	1.5	
Lyα	77	5	57.5	52.7	3.5	N	
Si IV	71	39	5.4	6.4	1.0	1.5	
C IV	63	12	52.5	49.8	5.1	5.7	
He II	58	31	9.9	7.9	1.6	1.2	
C III]	52	25	17.8	16.5	1.9	5.2	
Ratios of Equivalent Widths							
O VI/Lyα	50	24	0.12	0.12	0.02	0.03	
O VI/C IV	28	12	0.16	0.16	0.02	0.08	3
Si IV/Lyα	67	37	0.10	0.11	0.02	0.02	2
C IV/Lyα	59	10	0.81	0.84	0.06	N	2
He II/Lyα	54	27	0.16	0.13	0.02	0.02	3
C III]/Lyα	47	23	0.26	0.27	0.03	0.08	2
C III]/C IV	41	21	0.21	0.24	0.03	0.09	6
FWHM (km s^{-1})							
O VI	57	29	4570	4210	290	2250	
Lyα	77	5	7590	7690	250	3140	
Si IV	70	39	4790	4050	550	1240	
C IV	63	12	7940	7820	360	N	
C III]	52	25	5750	6340	520	N	

[a] All limits are upper limits except for α_{ox}
[b] Number of lower limits deleted from sample to allow analysis.

TABLE 6

BIVARIATE RESULTS[a]

Parameters Y	X	N_{total}	N_{limits} X low	X up	Y low	Y up	Both	P[b] (%)	Regression[c] Slope	Intercept	$N^{d}_{changed}$ X	Y
W_λ(Lyα)	l_{uv}	77	0	0	0	5	0	.01	-0.11 ± 0.05	5.2 ± 1.6	0	1
W_λ(Lyα)	α_{uv}	77	0	0	0	5	0	1.3	0.12 ± 0.06	1.9 ± 0.1	0	1
W_λ(Lyα)	α_{ox}	45	5	0	0	0	0	.17	-0.38 ± 0.23	2.3 ± 0.3	1	0
FWHM(Lyα)	l_{uv}	77	0	0	0	5	0	1.4	0.06 ± 0.01	2.1 ± 0.4	0	1
FWHM(Lyα)	α_{uv}	77	0	0	0	5	0	.01	-0.09 ± 0.03	$3.8 \pm .04$	0	0
W_λ(C IV)	l_{uv}	63	0	0	0	12	0	.02	-0.22 ± 0.05	8.3 ± 1.6	0	3
W_λ(C III])	l_{uv}	52	0	0	0	25	0	0.4	-0.27 ± 0.05	9.6 ± 1.5	0	9
W_λ(C III])	l_x	36	0	2	0	15	0	0.8	-0.19 ± 0.06	6.5 ± 1.6	0	6
C III]/Lyα	l_x	33	0	2	0	15	1	.03	-0.23 ± 0.10	5.6 ± 2.9	1	5
W_λ(He II)	l_{uv}	58	0	0	0	31	0	.01	-0.30 ± 0.07	9.9 ± 2.1	0	8
W_λ(He II)	l_x	37	0	3	0	17	0	.5	-0.27 ± 0.15	8.1 ± 4.1	0	5
He II/Lyα	l_{uv}	54	0	0	0	27	0	.7	-0.21 ± 0.08	5.5 ± 2.5	0	5
He II/Lyα	l_x	35	0	3	0	15	0	.7	-0.24 ± 0.31	5.7 ± 8.4	0	5

[a] Includes only parameter pairs with data for $N > 30$ QSOs and significant ($P < 2\%$) correlations in *both* generalized Spearman and Kendall's rank tests.

[b] Probability of achieving the Spearman-Rank correlation assuming the null hypothesis.

[c] Fits are from Schmitt's two-dimensional Kaplan-Meier regression to the logarithm of listed parameters (except for spectral slopes α_{UV} and α_{OX}.

[d] Outlying limits changed to detections at bin edges.

only marginally ($P < 6\%$), but has both slope and intercept consistent with previous results. The various adopted optical and X-ray k corrections make only small differences to the derived α_{OX}-values. More importantly, this correlation is found to be weak or possibly absent for log $l_{opt} \lesssim 31$ (Avni, Worrall, & Morgan 1995), which is close to the mean luminosity of our (and Corbin's) sample.

4.3. *Correlation of UV Emission Lines with SEDs*

We find several strong correlations ($P < 2\%$) between emission-line EW and continuum SED parameters. Comparing to luminosities, W_λ(Lyα), W_λ(C IV), W_λ(He II), and W_λ(C III]) all show significant anticorrelations with l_{UV}, i.e., a BEff. W_λ(He II) and W_λ(C III]) also correlate strongly with l_X. Since l_{UV} and l_X are very strongly correlated, these may be a secondary effect. To test for the primary relationship, we use the ASURV bivariate Spearman ranks as input to multivariate partial Spearman rank (PSR) analysis (Kendall & Stuart 1976). W_λ(C III]) correlates most strongly with l_X ($P_{PSR} = 0.059$, and a PSR of $\rho = -0.273$, while its correlation with l_{UV} has $P_{PSR} = 0.180$ and $\rho = -0.167$). The primary relationship of W_λ(He II) appears to be with l_{UV} ($P_{PSR} = 0.035$, $\rho = -0.310$ for l_{UV}; $P_{PSR} = 0.10$, $\rho = -0.216$ for l_X).

We also test a number of line *ratios* against SED parameters. The line ratio C III]/Lyα shows a significant correlation with X-ray luminosity. The ratio He II/Lyα depends similarly on both l_{UV} and l_X (see Table 6) but appears to be most sensitive to l_X ($P = 0.033$, $\rho = -0.322$ for l_X; $P = 0.278$, $\rho = -0.105$ for l_{UV}). These correlations are illustrated in Figure 1. Plots of W_λ versus X-ray luminosity appear similar, with slightly more scatter.

Testing the relationship of line W_λ with continuum *shape* parameters, we find a strong inverse correlation of W_λ(Lyα) with α_{OX} (Fig. 2). Since α_{OX} is known to increase with OUV luminosity, the anticorrelation between W_λ(Lyα) and α_{OX} could be a secondary effect. PSR tests do not reveal which of log l_{UV} or α_{OX} has the primary relationship to W_λ(Lyα)($P_{PSR} < 0.005$ for both). Simple substitution of the observed $\alpha_{OX}(l_{UV})$ relation into the observed W_λ(Lyα)(l_{UV}) relation found here produces a significantly steeper slope (~ -1) than we derive here for W_λ(Lyα)(α_{OX}). We suspect that this is a mathematical artifact of line regressions through a population with high dispersion, and with error in both variables. That a W_λ-to-α_{OX} correlation appears for Lyα but not other lines that show a BEff could be a result of the higher S/N of the Lyα line. We suspect that the W_λ(Lyα)-(α_{OX}) correlation is primary, however, since W_λ(Lyα) does

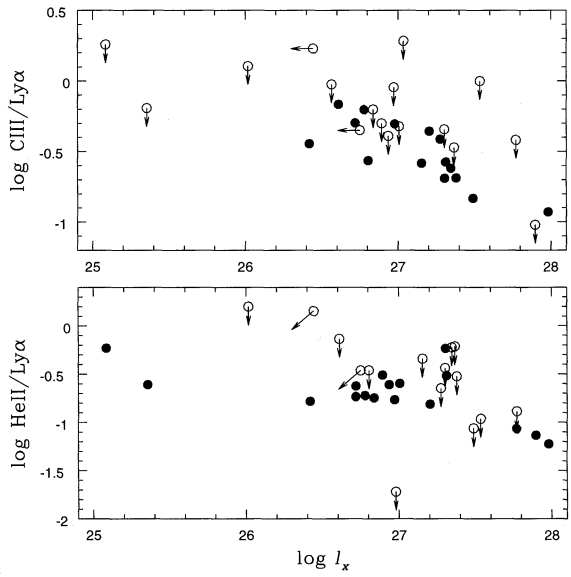

FIG. 1.—Line ratios (relative to Lyα) vs. X-ray luminosity for C III] and He II. Arrows denote upper limits to line ratios that, when tilted, are X-ray upper limits as well. Several very high upper limits are excluded in these plots, but these have no significance to the statistical results. Plots of W_λ vs. X-ray luminosity appear similar, with slightly more scatter.

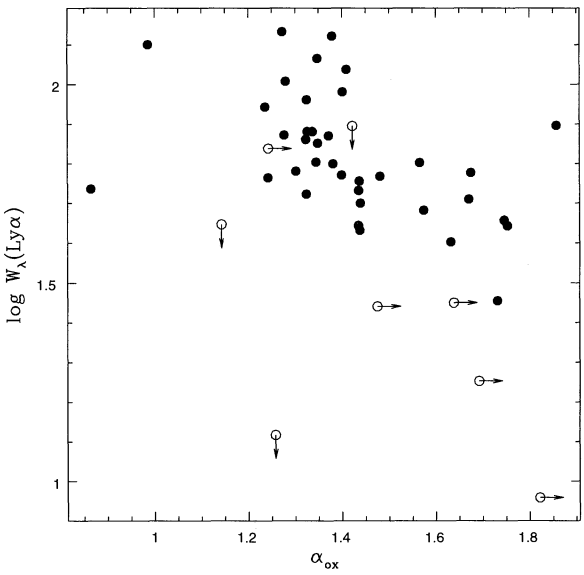

FIG. 2.—Lyα equivalent width vs. α_{ox}. Arrows denote limits. We find a strong inverse correlation of W_λ(Lyα) with α_{ox}. Since α_{ox} is known to increase with luminosity, the anticorrelation between W_λ(Lyα) and α_{ox} shown here could be a secondary effect. However, we do not observe an anticorrelation of W_λ(Lyα) with X-ray luminosity, as might be expected in such a case.

not correlate with X-ray luminosity l_X, and the latter clearly bears a stronger relationship to l_{UV} than does α_{ox}. We also point out that the trend in FWHM here could be strongly affected by changes in N v, or the Lyα/N v ratio.

We find few correlations between our measured line FWHM and SED parameters. However, FWHM(Lyα) correlates strongly to l_{UV} and to α_{UV}. Since α_{UV} and l_{UV} were from independent fits to the entire spectrum (LTS93), we expect that these trends are not an artifact of our choice of continuum used for line integration, which uses bands only redward of Lyα (Table 1). However, in data of such low S/N (the mean is about 8 for the *IUE* sample spectra), the FWHM measurements are not very robust. Asymmetry measurements, which require still higher moments of the flux distribution, are even less so, and are thus excluded from consideration here. We will construct composite spectra from subsamples with similar SEDs in a later paper to increase the overall S/N of these tests. This will be of particular use in incorporating the LBQS/RASS sample, for which X-ray flux stacking will permit an acceptable detection fraction (Green et al. 1995).

5. DISCUSSION

5.1. *Confirmations and New Results*

We confirm significant correlations between W_λ and UV luminosity (e.g., the well-studied Baldwin effect) for Lyα, C IV, He II, and C III]. Models of optically thick, geometrically thin accretion disks (Netzer 1987) have been successful in explaining several such line/continuum correlations. Limb darkening and projected surface area effects in these models call for a UV continuum flux that is strongest face-on and highly anisotropic compared to the harder (e.g., soft X-ray) ionizing flux. Quasar disks, particularly the area emitting the UV flux, are presumably much smaller than the BLR. Thus, a random selection of objects, differing only in disk inclination, results in measurements of constant line luminosities but yields UV continuum luminosities that vary with aspect, thereby producing the observed anticorrelation between W_λ and l_{UV}. We note that if indeed X-ray emission is more isotropic, much weaker correlations would be observed between W_λ and l_X. In addition, disks viewed face-on (smaller W_λ) would also appear to have boosted UV (larger α_{ox}). All of these predictions hold true in the current study for Lyα. However, within this geometric model, we would certainly expect to see the same set of correlations with C IV, yet there is no corresponding decrease of W_λ(C IV) with α_{ox}.

We report for the first time significant anticorrelations between W_λ(C III]), W_λ(He II), and X-ray luminosity that, for C III], appears to be primary. This correlation also seems to contradict the simplest geometrical explanation of the BEff. However, neither side of the argument may be physically meaningful unless we can contrast line W_λ to the continuum relevant to the line's production. For instance, C III] line emission should depend almost exclusively on the Lyman continuum (between about 13 and 25 eV), which is at least an order of magnitude in energy below the soft X-ray bandpass sampled here. He II line emission is spurred by continuum photons between 54 and 150 eV. UV lines such as Lyα and C IV, on the other hand, should also depend on energies (from 300–400 eV) closer to the *Einstein* bandpass (see Table 4 of Krolik & Kallman 1988, hereafter KK88).

Not only photons that serve to ionize the species in question contribute to emission-line production for that species. Ionization from excited states and heating via free-free and H^- absorption also help determine the line's principal ionizing/heating continuum (PIHC). Traditionally, the BEff is seen when comparing UV emission-line W_λ to UV luminosity. For some cases in the current study we are able to compare the line W_λ somewhat more directly to a portion of its PIHC using extant soft X-ray observations. For these cases, Lyα and C IV, the *X-ray* BEff is not significant. For He II and C III] lines, where the entire PIHC is softer than the *Einstein* bandpass (KK88), we show that a significant BEff persists relative to soft X-ray luminosities. This would suggest that the BEff weakens substantially when the continuum luminosity used for comparison to W_λ is close to the PIHC of the line. Changes in the relative normalization of the "near-line" continuum to the PIHC thus enhance the traditional BEff. This adds weight to previous arguments (beginning with Malkan & Sargent 1982) that the BEff is caused by changes in continuum shape. The increase in luminosity may primarily be caused by an increase in UV/EUV/soft X-ray emission (the BBB, possibly the thermal signature of an accretion disk) over the underlying power-law continuum. It has been proposed that the BBB shifts toward lower energies at higher (OUV) luminosities. This would entail (1) a strong increase in l_{UV}, (2) a weaker increase in l_X, and (3) an increase in α_{ox}. The response of line flux and W_λ depends in a fairly complicated manner on the relative peak energies of the BBB and the PIHC, and the BBB normalization relative to the power-law continuum. However, given adequate multiwavelength coverage, it is possible in principle to contrast the theoretical and observed line response.

In this picture, a stronger BEff might be expected for species of higher energy PIHC. Since traditionally, the BEff contrasts W_λ to the luminosity near the line, the slope or normalization of the BEff may be accentuated if the actual PIHC is more distant in energy from that luminosity. There

is indeed evidence for such a trend (Zheng, Feng, & Binette 1992; Espey, Lanzetta, & Turnshek 1993).

Another prediction of this picture is that lines in which PIHC is entirely observable will show a much weaker BEff relative to that continuum. Good candidates for such lines would have PIHCs very near the soft X-ray bandpass, with no contribution (as with Lyα and C IV) from softer continuum components. Some examples are observationally challenging: He I λ5876, with PIHC 300–500 eV, is quite weak; C II λ326, with PIHC above 800 eV, is in the EUV; O I λ8447 (PIHC > 600 eV) requires spectra at least into the near-IR for most QSOs. Space-based detection of Ne VIII λ774, which has an ionization energy of 207 eV, is difficult as well (Hamann et al. 1995). Study of other lines is more tractable: Fe II lines in the UV have their PIHC above 500 eV; Fe II lines in the optical are principally caused by continuum above 800 eV. There is some preliminary vindicating evidence that optical (λ4570) Fe II emission is intimately linked to its observable PIHC: Shastri et al. (1993) and Laor et al. (1994) found that QSOs with strong optical Fe II emission show softer (steeper) X-ray spectral slopes. Green et al. (1995) found that QSOs in the LBQS with strong UV Fe II emission (based on the iron feature under [Ne IV] λ2423) are anomalously X-ray bright in the *ROSAT* passband. To eschew any nascent complacency, we point out that Corbin (1993) did find an anticorrelation between W_λ(Fe II) and soft X-ray luminosity. Previous photoionization models may be insufficient in the case of Fe II, which (1) could partly arise from collisional excitation in regions optically thick to X-rays (e.g., Kwan & Krolik 1981) and (2) probably need drastically revised photoionization cross sections (Bautista & Pradhan 1995).

Mg II λ2798 appears to be the best candidate for testing our predictions. This line has a PIHC between 600–800 eV, and is much more easily and objectively measured than are the broad Fe II multiplets. Studies of Mg II emission lines versus X-ray continuum appear to have been overlooked. Though an insufficient number of *IUE* spectra in this study include the Mg II region, we are currently pursuing such correlations with the LBQS/RASS sample (Green et al. 1996).

The line ratios C III]/Lyα and He II/Lyα both show their strongest dependence on l_X. KK88 state that, since pure recombination is a poor approximation for Lyα in broad-line clouds, the He II/Lyα line ratio can trace only very large spectral contrasts in the continuum. In fact, neither of these lines shows a strong correlation across a wide range of α_{OX}. By contrast, Boroson & Green (1992) found an anticorrelation between He II λ4686/Hβ and α_{OX}. This may indicate that no simple relation exists between the optical and UV helium line strengths. Boroson & Green had pointed out the potential utility such a relation might hold for luminosity calibration and measurements of q_0.

5.2. *Nonconfirmations of Previous Results*

We do *not* confirm the correlation of O VI/Lyα with α_{OX} reported by ZKD. They also find strong anticorrelations between W_λ(O VI) and both α_{OX} (slope -0.81 ± 0.27) and log l_{UV} (slope -0.30 ± 0.03). Using our *IUE* sample, and including upper limits, we cannot confirm any of these correlations at our adopted significance level (see Fig. 3). However, when we analyze *detections only*, we find significant correlations, with slopes consistent with ZKD (-0.81 ± 0.30 and -0.41 ± 0.08, respectively). These

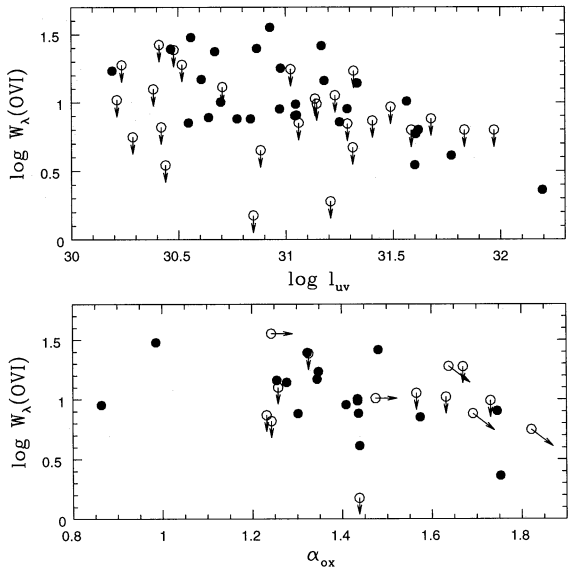

FIG. 3.—O VI] equivalent width vs. UV luminosity and α_{OX}. Arrows denote limits. Contrary to Zheng et al. (1995), we do not confirm significant ($P < 2\%$) correlations between W_λ(O VI) and either α_{OX} or log l_{UV} from our *IUE* sample. However, when we analyze *detections only*, we find significant correlations, with slopes consistent with Zheng et al. (-0.81 ± 0.30 and -0.41 ± 0.08, respectively). This illustrates that the exclusion of undetected lines from line/continuum studies may spuriously enhance apparent correlations.

results highlight that *upper limits should always be included to avoid spuriously significant line/continuum correlations.* However, the ZKD result is still valid—they appear to have detected O VI for every QSO in their sample a posteriori (e.g., the sample was not selected for strong O VI emission). Some of the correlations seen by ZKD and others are probably indeed intrinsic to QSOs, but are not reproduced here because of the smaller luminosity range of our sample. This will be tested in an upcoming paper, which includes a larger luminosity range while still including limits. (However, to avoid contamination of the O VI line region by Lyα forest absorption, we will still be limited to relatively low redshifts. Future inclusion of *HST* data is clearly warranted, but beyond the scope of the current study.) We note also that 27 of 32 of the QSOs in the ZKD sample are radio-loud, for which the BEff may be enhanced (perhaps a bias introduced by their greater variability; Murdoch 1983). Zamorani et al. (1992) discuss these issues further, and find flatter slopes in W_λ(C IV) versus l_{UV} using optically selected QSOs than were found in the PKS sample of Baldwin et al. (1989). The slope we find here is intermediate.

The early single cloud models of Mushotsky & Ferland (1984) first suggested that the observed increase of α_{OX} with luminosity could cause the BEff, and would also predict, if anything, a *negative* correlation of C IV/Lyα with luminosity. Baldwin et al. (1989, hereafter BWG) and Kinney et al. (1987, 1990) found that both C IV/Lyα and C III]/C IV are inversely correlated with UV luminosity. We confirm neither of these correlations. The same single cloud models also predicted that Lyα, C IV, and C III] line ratios should be relatively independent of both α_{OX} and α_X because these lines should not originate from X-ray–heated zones deeper in the emission-line clouds. Here we find instead that W_λ(Lyα) does depend an α_{OX}, and that C III]/Lyα anticorrelates with X-ray luminosity.

Optically thin clouds, which may become fully ionized in hydrogen (Goad, O'Brien, & Gondhalekar 1993; Shields, Ferland, & Peterson 1995), may also demand inclusion in models of the BLR. The response of line emission to continuum changes may be flat or even negative in optically thin clouds, which can help reproduce (1) the observed difference in the lag of the high- and low-ionization lines relative to the continuum in Seyferts (e.g., Reichert et al. 1994); (2) some ultraviolet absorption features and "warm absorber" behavior in the X-ray regime (e.g., Mathur 1994); and (3) the intrinsic BEff. The latter is a strong decrease in line equivalent width that occurs as the luminosity increases in individual variable Seyferts (Kinney et al. 1990). The global BEff has a much shallower slope, which might be explained by a decrease in the covering factor f_c of the optically thin component, owing to more efficient outflow of thin clouds in intrinsically brighter sources.

We briefly explore reasons why several correlations between line and continuum parameters that have been found significant in other studies are not reproduced here. (1) Some studies, while more heterogeneous, have embraced a wider luminosity range than our *IUE* sample, often including optical data and higher redshift QSOs. Several results (e.g., Wampler et al. 1984; Kinney et al. 1987) have shown that for QSOs of lower luminosity ($\log l_{\rm UV} \lesssim 31$), the W_λ-luminosity relations flatten or disappear. The mean $\log l_{\rm UV}$ of the *IUE* sample we investigate here is 30.6, with only about a third of the sample having $\log l_{\rm UV} > 31$. Even at higher luminosities, a very large range of luminosity is often required to overcome intrinsic scatter in the global Baldwin relation, and scatter induced by variability (e.g., Kinney et al. 1990). (2) The exclusion of undetected emission lines from many previous samples spuriously enhances the apparent statistical significance of line/continuum correlations. We note that a slight relaxation of our significance criterion from $P < 2\%$ to $P \lesssim 5\%$ would have retrieved several previously reported correlations. (3) Although the *IUE/Einstein* sample is large, and the data and analysis homogeneous, the QSOs therein were selected for observation by these satellites for a variety of reasons, so this sample cannot be considered truly complete or homogeneous.

6. CONCLUSIONS

Complex activity is likely to be associated with the nuclear environment in QSOs. Rapid star formation and evolution, supernovae, accretion/merging of galaxies or protogalactic fragments, and a supermassive accreting black hole may all contribute. Although QSO spectra are surprisingly homogeneous given such a flamboyant cast, the simplest geometric and photoionization models do not succeed in explaining the relationship of QSO emission lines to the observed continuum. This may partly be alleviated if the line emission can be directly compared to its principal ionizing/heating continuum.

Objective, automated line measurements including line upper limits are crucial to avoid spurious enhancement of apparent line/continuum correlations. We find significant correlations between W_λ and UV luminosity (e.g., the well-studied Baldwin effect) for Lyα, C IV, He II, and C III]. W_λ(C III]) and W_λ(He II) also show previously unreported correlations with X-ray luminosity that, for C III], appears to be primary. The line ratios C III]/Lyα and He II/Lyα both show strongest dependence on $l_{\rm X}$. W_λ(Lyα) correlates strongly with spectral slopes $\alpha_{\rm UV}$ and $\alpha_{\rm OX}$ (between 2500 Å and 2 keV), but *not* with X-ray luminosity.

Using these results, we argue that one simple geometrical interpretation of the BEff that assumes ionizing X-ray emission to be more isotropic than UV continuum emission is not plausible. If indeed the BEff were a result of a distribution of disk inclinations in this case, weak anticorrelations of line W_λ with X-ray luminosity would be expected at best. The significant anticorrelations of C III] and He II emission with $l_{\rm X}$ thus render the simplest geometrical model unlikely.

When we are able to compare the line W_λ most directly to a portion of its PIHC using extant soft X-ray observations (for Lyα and C IV) the *X-ray* BEff is not significant. For He II and C III] lines, where the entire PIHC is softer than the *Einstein* bandpass (KK88), a significant BEff persists relative to soft X-ray luminosities. We thus argue that the BEff weakens or disappears when the line emission is compared to the luminosity in the bandpass of its principle photoionizing continuum. This supports an interpretation of the BEff as a change in spectral energy distribution with luminosity. We predict that no BEff relative to soft X-ray luminosity should be found for Fe II or Mg II emission lines. Extensions of our method to samples of a wider redshift/luminosity range would test these predictions.

Now that we have outlined a technique for the efficient measurement of large numbers of comparatively low-S/N QSO spectra, we will apply it to the largest, most uniformly selected such sample to date, the LBQS. Optical spectra and X-ray fluxes or upper limits are available for 908 QSOs in the LBQS from the *ROSAT* All-Sky Survey. Analysis of that database will be combined with the results presented here to offer a truly wide luminosity baseline for further study of the interdependence of QSO continuum and emission-line properties.

Of course, we would have preferred for each line an accurate measure of its rest-frame principle ionizing/heating continuum. For O VI, this means the "He I continuum" (24.5–54.4 eV). For Lyα C III] and C IV this means the ranges 13.6–24.5 eV (the "Lyman continuum") dominates (KK88). C III] and C IV should depend also on ionizing photons from 0.3–0.4 keV. Since these include the EUV range, which is observationally inaccessible for all but a handful of nearby AGNs (Marshall, Fruscione, & Carone 1995), we have attempted an indirect examination of the relevant continuum via the adjacent UV and X-ray luminosities, and through $\alpha_{\rm OX}$. The true strength of the EUV is best estimated using spectral index and normalization in the adjacent UV and soft X-ray bands together. Slopes are available in the UV data set, but the great majority of X-ray data provide only net counts in the *Einstein* bandpass ($\sim$0.16–3.5 keV). Unfortunately, there are too few QSOs in the *IUE* sample with published $\alpha_{\rm X}$ (about 18, judging from Elvis et al. 1994) to permit any convincing statistical tests. The 2 keV monochromatic fluxes used in $\alpha_{\rm OX}$ are thus derived from these *Einstein* counts assuming a single power-law slope and absorption due to Galactic $N_{\rm H}$ only. Although there may be absorption (either warm or cold; see, e.g., Netzer 1993) intrinsic to the QSOs, this effect is unlikely to be strong. A small soft excess above the power law, which could be important to the ionizing continuum is, however, expected in many of the QSOs (Fiore et al. 1994). Estimates of X-ray spectral slopes in the *ROSAT* band (0.1–2.4 keV) for more than 100 bright QSOs should be available from *ROSAT* observations within the next few years (e.g.,

Bade et al. 1995). These data should prove a valuable addition to the studies initiated here.

Hearty thanks to Ken Lanzetta for providing his *IUE* spectral atlas, including error spectra and continuum fits, in digital form. Paul Eskridge helped simplify the task of PSR analysis. Craig Foltz provided a copy of the LBQS composite spectrum. I gratefully acknowledge Avi Loeb for our discussions of the emission-line error analysis. The author gratefully acknowledges support provided by NASA through grant NAG 5-1253, as well as HF-1032.01-92A awarded by the Space Telescope Science Institute, which is operated by the Association of Universities for Research in Astronomy, Inc., under NASA contract NAS 5-26555.

APPENDIX A

DEFINITIONS OF THE LINE PARAMETERS

Following Robertson (1986), the line equivalent width, W_λ, is

$$W_\lambda = \sum_{i=\lambda_1}^{\lambda_2} \left(\frac{f_{l,i}}{f_{c,i}} - 1\right)\Delta\lambda_i \,, \tag{A1}$$

where $f_{l,i}$ and $f_{c,i}$ represent the flux in the line and continuum, respectively, at the ith pixel.

The FWHM, δ is taken to be

$$\mathrm{FWHM}_\lambda = 1.1775(\Lambda_H - \Lambda_L) \,. \tag{A2}$$

Here Λ_H and Λ_L are the wavelengths where 16% and 84% of the line flux, respectively, are reached while integrating over the line region, corresponding to the $\pm 1\ \sigma$ points for a (noise-free) Gaussian line profile. These wavelengths are defined by the following equations:

$$\sum_{-\infty}^{\Lambda_L} \left(\frac{f_{l,i}}{f_{c,i}} - 1\right)\Delta\lambda = 0.1587 W_\lambda$$

and

$$\sum_{-\infty}^{\Lambda_H} \left(\frac{f_{l,i}}{f_{c,i}} - 1\right)\Delta\lambda = 0.8413 W_\lambda .$$

The definition of the asymmetry parameter, ξ, is

$$\xi = \frac{100}{\delta}\left[0.5(\Lambda_H + \Lambda_L) - \Lambda\right] . \tag{A3}$$

Here Λ is the median wavelength, where 50% of the line flux is reached while integrating over the line region:

$$\sum_{-\infty}^{\Lambda} \left(\frac{f_{l,i}}{f_{c,i}} - 1\right)\Delta\lambda = 0.5 W_\lambda .$$

APPENDIX B

ERROR COMPUTATIONS FOR LINE PARAMETERS

B1. ERRORS ON THE WAVELENGTHS Λ,Λ_L, Λ_H

The error in Λ is

$$\sigma_\Lambda^2 = \left(\frac{\partial\Lambda}{\partial W_\lambda}\right)^2 \sigma_{W_\lambda}^2 \approx \frac{\sigma_{W_\lambda}^2}{(dW_\lambda/d\Lambda)^2} \,.$$

Recalling that if

$$y = \int_{-\infty}^{a} f(x)dx \,,$$

then $\partial y/\partial a = f(\mathrm{a})$, and so

$$\frac{dW_\lambda}{d\Lambda} = \frac{1}{0.5}\left(\frac{f_l - f_c}{f_c}\right)_\Lambda . \tag{B1}$$

Thus,

$$\sigma_{\Lambda}^2 = \left(\frac{0.5 f_c}{f_l - f_c}\right)_{\Lambda}^2 \sigma_{W_\lambda}^2 .$$

Similarly,

$$\sigma_{\Lambda_L}^2 = \left(\frac{0.1587 f_c}{f_l - f_c}\right)_{\Lambda_L}^2 \sigma_{W_\lambda}^2 ,$$

and

$$\left(\frac{0.8413 f_c}{f_l - f_c}\right)_{\Lambda_H}^2 \sigma_{W_\lambda}^2 .$$

B2. ERRORS ON LINE PARAMETERS W_λ, δ, AND ξ

Propagation of errors from equation (A1) yields, for a single pixel in the line,

$$\sigma_{W_{\lambda,i}}^2 = \left[\left(\frac{1}{f_{c,i}}\right)^2 \sigma_{l,i}^2 \Delta + \left(\frac{f_{l,i}}{f_{c,i}^2}\right)^2 \sigma_{c,i}^2\right] \Delta\lambda_i^2 .$$

Since our continuum level is fitted from a large number of points, its formal error should be low. We nevertheless conservatively assume that the error in the continuum across the line region $\sigma_{c,i}$ is equal to the error in the signal itself $\sigma_{l,i}$. Thus, we estimate the variance in the equivalent width to be

$$\sigma_{W_\lambda}^2 = \sum_{i=\lambda_1}^{\lambda_2} \left[\left(\frac{1}{f_{c,i}}\right)^2 + \left(\frac{f_{l,i}}{f_{c,i}^2}\right)^2\right] \sigma_{l,i}^2 (\Delta\lambda_i)^2 . \tag{B2}$$

When σ_l is not directly available from a 1 σ error spectrum, we estimate it from the mean variance $\overline{\sigma_c^2}$ in the continuum bands as $\sigma_{l,i}^2 = \overline{\sigma_c^2}(f_{l,i}/f_{c,i})$. Tests show that this substitution yields error estimates generally within about 30% of those obtained using the actual 1 σ error spectra.

Propagation of errors for equation (A2) yields a variance in FWHM of

$$\sigma_\delta^2 = 1.1775^2 (\sigma_{\Lambda_H}^2 + \sigma_{\Lambda_L}^2) ,$$

For the variance in the asymmetry parameter, propagation of errors for equation (A3) yields

$$\sigma_\xi^2 = \frac{1}{\delta^2} \left[(1.1775^2 \xi^2 + 50^2)(\sigma_{\Lambda_H}^2 + \sigma_{\Lambda_L}^2) + 100^2 \sigma_\Lambda^2\right] .$$

REFERENCES

Avni, Y., Worrall, D. M., & Morgan, W. A., Jr. 1995, ApJ, 454, 673
Bade, N. Fink, H. H., Engels, D., Voges, W., Hagen, H.-J., Wisotzki, L., & Reimers, D. N. 1995, A&AS, 110, 469
Baldwin, J. A. 1977, ApJ, 214, 679.
Baldwin, J. A., Ferland, G., Korista, K., & Verner, D. 1996, ApJ, 455, L119
Baldwin, J. A., Wampler, E. J., & Gaskell, C. M. 1989, ApJ, 338, 630(BWG)
Barvainis, R. 1993, ApJ, 412, 513
Bautista, M. A., & Pradhan, A. K. 1995, At. Mol. Opt. Phys., 28, L173
Binette, L., Prieto, A., Szusziewicz, E., & Zheng, W. 1989, ApJ, 343, 135
Boroson, T. A., & Green, R. F. 1992, ApJS, 80, 109
Brotherton, M. S., Wills, B. J., Steidel, C. C., & Sargent, W. L. W. 1994, ApJ, 423, 131
Clavel, J., et al. 1992, ApJ, 393, 113
Corbin, M. R. 1992, ApJ, 391, 577
———. 1993, ApJ, 403, L9
Corbin, M. R., & Francis, P. J. 1994, AJ, 108, 2016
Cristiani, S., & Vio, R. 1990, A&A, 227, 385
Elvis, M., et al. 1994, ApJS, 95, 1
Espey, B. R., Lanzetta, K. M., & Turnshek, D. A. 1993, BAAS, 25, 1448
Ferland, G. F., & Shields, G. A. 1985, in Astrophysics of Active Galaxies and Quasi-stellar Objects, ed. J. Miller (Mill Valley: University Science Books), 57
Fiore, F., Elvis, M., McDowell, J. C., Siemiginowska, A., & Wilkes, B. J. 1994, ApJ, 431, 515
Francis, P. J., Hewett, P., Foltz, C., Chaffee, F., Weymann, R., & Morris, S. 1991, ApJ, 373, 465
Goad, M. R., O'Brien, P. T., Gondhalekar, P. M. 1993, MNRAS, 263, 149
Green, P. J., & Mathur, S. 1996, ApJ, 462, 637
Green, P. J., Schartel, N., Anderson, S. F., Hewett, P. C., Foltz, C. B., Fink, H., Brinkmann, W., Trümper, J., & Margon, B. 1995, ApJ, 450, 51
Green, P. J., et al. 1996, in preparation
Hamann, F., Shields, J. C., Ferland, G. J., & Korista, K. T. 1995, ApJ, 454, 688
Hayes, D. S., & Latham, D. W. 1975, ApJ 197, 599
Hewitt, A., & Burbidge G. 1993, ApJS, 87, 51 (HB93)
Kendall, M., & Stuart, A. 1976, The Advanced Theory of Statistics, Vol. II (New York: Macmillan)
Kinney, A. L., Huggins, P. J., Glassgold, A. E., & Bregman, J. N. 1987, ApJ, 314, 145
Kinney, A. L., Rivolo, A. R., & Koratkar, A. P. 1990, ApJ, 357, 338
Krolik, J. H., & Kallman, T. R. 1988, ApJ, 324, 714 (KK88)
Kwan, J., & Krolik, J. H. 1981, ApJ, 250, 478
Lanzetta, K. M., Turnshek, D. A., & Sandoval, J. 1993, ApJS, 84, 109 (LTS93)
Lanzetta, K. M., Wolfe, A. M., & Turnshek, D. A. 1995, ApJ, 440, 435
Laor, A., Bahcall, J. N., Jannuzi, B. T., Schneider, D. P., Green, R. F. 1995, ApJS, 99, 1
Laor, A., Fiore, F., Elvis, M., Wilkes, B. J., & McDowell, J. 1994, ApJ, 435, 611
LaValley, M., Isobe, T., & Feigelson, E. D. 1992, in Astronomical Data Analysis Software & Systems, ed. D. Worrall et al. (San Francisco: ASP)
Malkan, M., & Sargent, W. L. W. 1982, ApJ, 254, 22
Marshall, H. L., Fruscione, A., & Carone, T. E. 1995, ApJ, 439, 90
Masnou, J.-L., Wilkes, B. J., Elvis, M., Arnaud, K. A., & McDowell, J. C. 1992, A&A, 253, 35
Mathur, S. 1994, ApJ, 431, L75
Murdoch, H. S. 1983, MNRAS, 202, 987
Mushotzky, R. F., & Ferland, G. J. 1984, ApJ, 278, 558
Netzer, H. 1987, MNRAS, 225, 55
———. 1993, ApJ, 411, 594
Pogge, R. W., & Peterson, B. M. 1992, AJ, 103, 1084
Reichert, G. A., et al. 1994, ApJ, 42, 582
Robertson, J. G. 1986, PASP, 98, 1220
Schartel, N., Green, P. J., Anderson, S. F., Hewett, P. C., Fink, H., Brinkmann, W., Trümper, J., Margon, B., & Foltz, C. B. 1996, MNRAS, submitted
Shastri, P., Wilkes, B. J., Elvis, M., & McDowell, J. 1993, ApJ, 410, 29
Shields, J. C., Ferland, G. J., & Peterson, B. M. 1995, ApJ, 441, 507

Steidel, C. C., & Sargent, W. L. W. 1991, ApJ, 382, 433
Tananbaum, H., Avni, Y., Green, R. F., Schmidt, M., & Zamorani, G. 1986, ApJ, 305, 57
Turner, T. J., & Pounds, K. A. 1989, MNRAS, 240, 833
Tytler, D., & Fan, X.-M. 1992, ApJS, 79, 1
Wampler, E. J., Gaskell, C. M., Burke, W. L. , & Baldwin, J. A. 1984, ApJ, 276, 403
Wang, T., Brinkmann, W., & Bergeron, J. 1996, A&A, in press
Weymann, R. J., et al. 1991, ApJ, 373, 23
Wilkes, B. J., & Elvis, M. 1987, ApJ, 323, 243
Wilkes, B. J., Tananbaum, H., Worrall, D. M., Avni, Y., Oey, M. S., & Flanagan, J. 1994, ApJS, 92, 53 (WEA94)
Zamorani, G., Marano, B., Mignoli, M., Zitelli, V., & Boyle, B. J. 1992, MNRAS, 256, 238
Zheng, W. 1991, ApJ, 382, L55
Zheng, W., Fang, L. Z., & Binette, L. 1992, ApJ, 392, 74
Zheng, W., Kriss, G. A., & Davidsen, A. F. 1995, ApJ, 440, 606 (ZKD)
Zheng, W., & Malkan, M. A. 1993, ApJ, 415, 517